Chemical Vapor Deposited Monolayer MoS_2 Top-Gate MOSFET with Atomic-Layer-Deposited ZrO_2 as Gate Dielectric

Yaoqiao Hu[1], Huaxing Jiang[1], Kei May Lau[1,2], and Qiang Li[1,2,*]

[1] Department of Electronic and Computer Engineering, Hong Kong University of Science and Technology (HKUST), Clear Water Bay, Kowloon, Hong Kong
[2] Institute for Advanced Study (IAS), Hong Kong University of Science and Technology (HKUST), Hong Kong

Corresponding author: Qiang Li. Email: eeqli@ust.hk

***Abstract*—**For the first time, ZrO_2 dielectric deposition on pristine monolayer MoS_2 by atomic layer deposition (ALD) is demonstrated and ZrO_2/MoS_2 top-gate MOSFETs have been fabricated. ALD ZrO_2 overcoat, like other high-*k* oxides such as HfO_2 and Al_2O_3, was shown to enhance the MoS_2 channel mobility. As a result, an on/off current ratio of over 10^7, a subthreshold slope (*SS*) of 276 mV/dec, and a field-effect electron mobility of 12.1 $cm^2 \cdot V^{-1} \cdot s^{-1}$ have been achieved. The maximum drain current of the MOSFET with a top-gate length of 4 μm and a source/drain spacing of 9 μm is measured to be 1.4 μA/μm at V_{DS} = 5 V. The gate leakage current is below 10^{-2} A/cm^2 under a gate bias of 10 V. A high dielectric breakdown field of 4.9 MV/cm is obtained. Gate hysteresis and frequency-dependent capacitance-voltage measurements were also performed to characterize the ZrO_2/MoS_2 interface quality, which yielded an interface state density of ~3×10^{12} $cm^{-2}eV^{-1}$.

Keywords: Atomic layer deposition, ZrO_2, MoS_2, top-gate transistor

I. INTRODUCTION

With a sizable bandgap that changes from indirect to direct in single layers, semiconducting two-dimensional molybdenum disulfide (MoS_2) has recently gained tremendous interest for transistors, photodetectors and electroluminescent devices [1-3]. Thanks to the enhanced electrostatic control of the gate over the channel [2-4], MoS_2 field effect transistors (FETs) have demonstrated outstanding device performance, such as high on/off current ratios up to 10^8 [2-3], a near-ideal subthreshold swing of 60 mV/dec [3-4], and good carrier mobilities [5]. To increase the gate capacitance and preserve a high channel mobility through the dielectric screening effect [6], integration of high-*k* technology with MoS_2 transistors is essential. However, atomic-layer deposition (ALD) of high-quality gate dielectrics on 2D materials has proven challenging [7-10] because of the lack of surface-dangling bonds.

The high-*k* dielectrics investigated to date include TiO_2, $SrTiO_3$, Al_2O_3, HfO_2, ZrO_2, and the associated silicates [11-15]. Among these, Al_2O_3, HfO_2, and ZrO_2 have been widely studied and are believed to be the most promising candidates due to their high dielectric constant, good thermodynamic stability, and reasonable band gap [16, 17]. Although Al_2O_3 and HfO_2 have been intensely used to fabricate MoS_2 top-gate transistor [18, 19], ZrO_2 is, to the best of our knowledge, only reported in back-gate transistors [20]. By transferring MoS_2 flakes onto a pre-deposited high-k dielectric layer, the back-gate approach bypasses the challenges associated with ALD deposition on 2D materials. However, there would remain significant interest in readily using the chemical vapor deposition (CVD) grown MoS_2 films to build top gate transistors which are more in line with mainstream transistor design and integration.

Previous studies on high-*k*/MoS_2 based top-gated transistors have almost exclusively been focused on mechanically exfoliated flakes. However, due to the small size of few-layer films and

possible extraneous contamination from exfoliation process, mechanical exfoliation is not a scalable or reproducible method for commercial use [21]. New synthetic routes such as CVD allow for both high-quality and large-area thin films. In fact, a variety of 2D materials including graphene [22], boron nitride [23] and MoS_2 [24] have reportedly been synthesized by CVD methods. However, the electrical properties of CVD MoS_2, especially the device performances of top-gated transistors, have not been comprehensively studied.

In this work, we report the first realization of CVD monolayer MoS_2 top-gate transistors with ALD ZrO_2 as gate dielectric. Using a low-temperature ALD process, we achieve direct deposition of ZrO_2 on pristine monolayer MoS_2. The fabricated top-gate transistors exhibit well-behaved characteristics with high on/off current ratios and low gate leakage current. The influence of ALD ZrO_2 on the electrical performance of MoS_2/SiO_2 back-gate transistor is discussed. The dielectric properties, as well as the MoS_2/ZrO_2 interface quality have been investigated.

II. EXPERIMENTAL DETAILS

Fig. 1(a) displays a cross-section schematic of the MoS_2 MOSFET with a top-gate electrode. A top-view optical microscope image of a fabricated device is shown Fig. 1(b). Monolayer MoS_2 reported in this work were grown by chemical vapor deposition on a heavily doped Si substrate capped with 300 nm SiO_2. High purity MoO_3 and S powder were used as precursors. The as-grown single-crystal [25] triangular shaped MoS_2 (with average edge length ~40 μm) was characterized by Raman scattering. As shown by the Raman spectrum in Fig. 1(c), the frequency difference between the in-plane (E^1_{2g}, ~385.1 cm^{-1}) and out-of-plane (A_{1g}, ~405.1 cm^{-1}) phonon modes confirms that the deposited MoS_2 is of monolayer thickness [26]. The device fabrication started with deposition of source/drain (S/D) electrodes (10/90 nm Ti/Au) by standard

lithographic patterning. ZrO_2 was then deposited directly on the MoS_2 films in an Oxford OpAL ALD reactor at a temperature of 200 °C. Tetrakis ethylmethylamino zirconium (TEMAZ) and water were used as precursors. After 300 ALD cycles, ~27 nm ZrO_2 was deposited and confirmed by ellipsometry measurement. Subsequently, source/drain contact holes were opened using a combination of dry and wet etching of the ZrO_2 layer. Finally, gate metal (10/90 nm Ti/Au) was defined. A dimension 3100 AFM system was used to examine the surface morphology after ALD deposition. All electrical tests were carried out using an Agilent 4156C precision semiconductor parameter analyzer at room temperature.

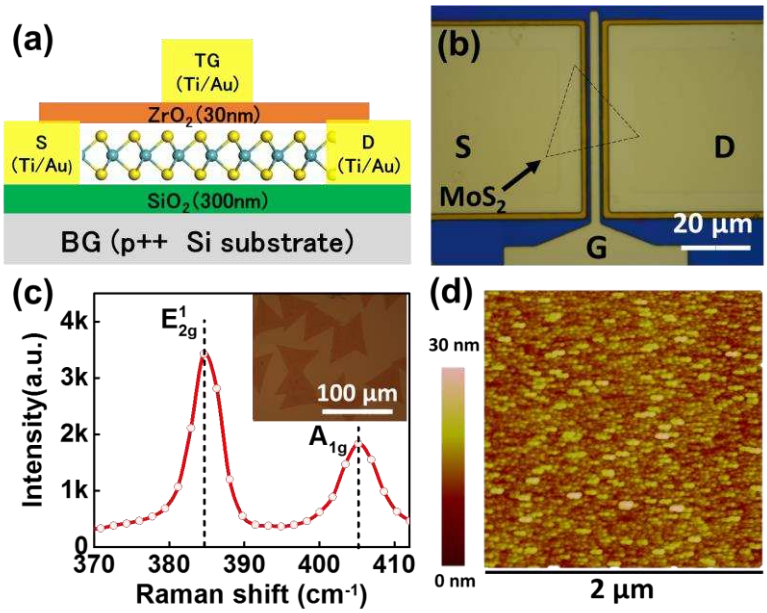

FIG. 1. (a) Schematic illustration of a monolayer ZrO_2/MoS_2 top-gate field-effect transistor. The p++ Si substrate acts as global back gate (BG) while Ti/Au metal stack as top gate (TG). (b) Optical microscope image of a typical MoS_2 device. (c) Raman spectrum of the as-grown MoS_2 film on Si/SiO_2 substrate measured at room temperature. Laser wavelength for Raman measurement is 514 nm. The inset shows the optical image of monolayer MoS_2 on SiO_2/Si substrate. (d) AFM image of the ALD-ZrO_2 on MoS_2.

III. RESULTS AND DISCUSSION

Fig. 1(d) shows a representative AFM image of the surface of the atomic-layer-deposited ZrO_2 on single-layer MoS_2. The ZrO_2 is continuous but exhibits island type morphology [27]. A root

mean square (RMS) roughness of 2.95 nm was obtained across a scanning area of 2×2 μm^2. This surface roughness is inferior when compared with the optimized ALD deposition of Al_2O_3 on MoS_2 (0.58 nm in rms for Al_2O_3 on MoS_2 [28]) and needs to be further optimized. The roughness could undermine the mobility of MoS_2 underneath and cause gate leakage fluctuations. Nevertheless, microscope observations indicated a complete coverage of direct ALD on pristine MoS_2, which is attributed to physical absorption of precursors on the basal plane. This is also observed in previous demonstrations of ALD Al_2O_3 [10] and HfO_2 [27] on MoS_2 at the optimized temperature window.

We first discuss the influence of ALD ZrO_2 overcoat on the electrical performance of CVD monolayer MoS_2/SiO_2 back-gate transistor. Fig. 2 shows the transfer and output characteristics of a ZrO_2/SiO_2 back-gate FET before and after the deposition of ZrO_2. Previous studies have shown that high-k oxides HfO_2 and Al_2O_3 encapsulation can greatly improve the MoS_2 channel mobility through Coulomb scattering screening effect. [6] In our case, the device shows more than doubled drive current after ZrO_2 deposition, implying mobility improved by ZrO_2 overcoating which is similar to HfO_2 and Al_2O_3. The field-effect mobility is extracted from the I_D versus V_{bg} curves in the linear region by using the expression $\mu = L/V_{DS}C_{ox} \times (dI_{DS}/dV_{bg})$, where L and W are the channel length and width, V_{DS} is the source-drain voltage, and C_{ox} is the back-gate capacitance per unit area. At room temperature, the extracted mobility before and after ZrO_2 top dielectric are 6.9 $cm^2V^{-1}s^{-1}$ and 11.5 $cm^2V^{-1}s^{-1}$, respectively. We attribute the mobility enhancement to the suppressed charged impurity scattering, which is similar to the Al_2O_3/MoS_2 and HfO_2/MoS_2 top-gate transistors. [6, 18] The mobility with ZrO_2 overcoating is not as high as that of the best transistor using HfO_2 [7] as the gate dielectric, which is possibly attributed to the large Coulomb scattering from fixed charges near the ZrO_2 surface induced by the comparatively

lower ALD deposition temperature [29]. In addition, we observe that while our device was intrinsically n-doped (a negative bias voltage required to reach neutral point) for both before and after ALD growth, the threshold voltage was positively shifted after the ZrO_2 deposition. The reason for this shift is not clear and is still under investigation.

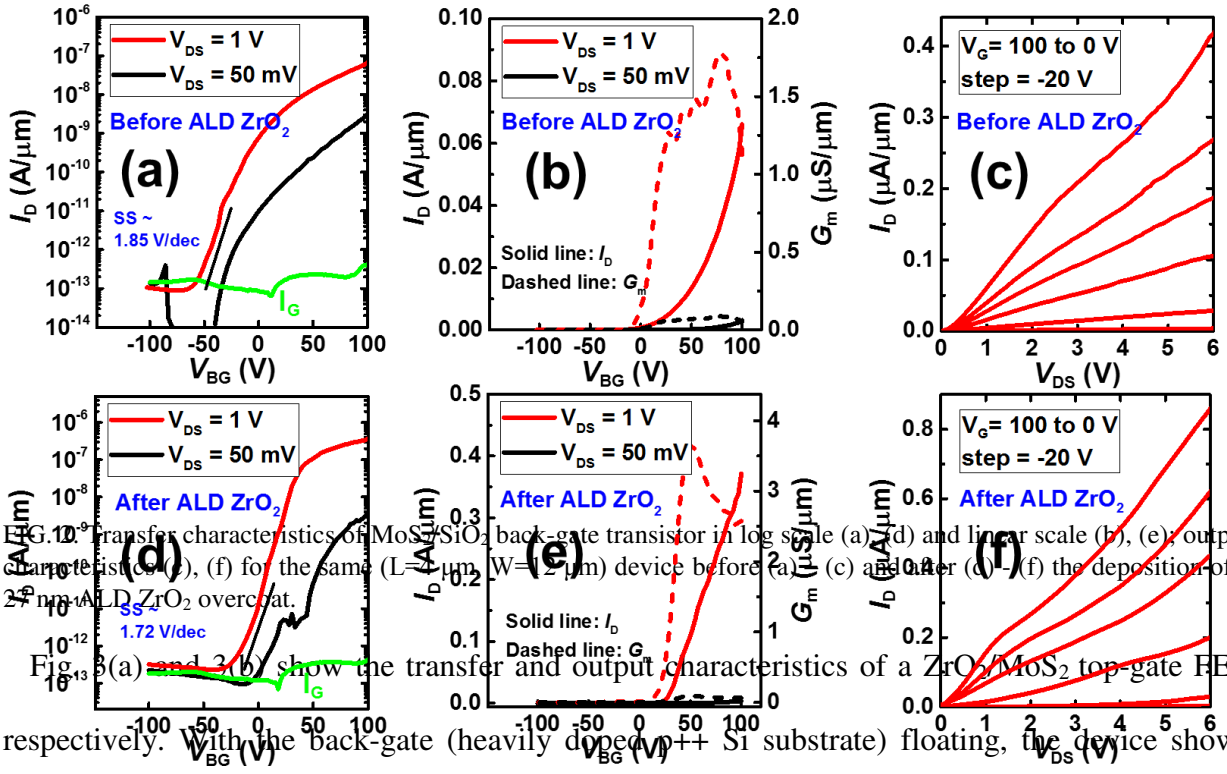

FIG. 2. Transfer characteristics of MoS_2/SiO_2 back-gate transistor in log scale (a), (d) and linear scale (b), (e); output characteristics (c), (f) for the same (L=4 μm, W=12 μm) device before (a), (c) and after (d) - (f) the deposition of a 27 nm ALD ZrO_2 overcoat.

Fig. 3(a) and 3(b) show the transfer and output characteristics of a ZrO_2/MoS_2 top-gate FET respectively. With the back-gate (heavily doped n++ Si substrate) floating, the device shows typical n-type conduction behavior and an on/off current ratio of ~10^6. At V_{DS} = 5V, the subthreshold slope (*SS*) is 276 mV per decade. The relatively large *SS* can be attributed to the un-optimized MoS_2/ZrO_2 interface. Furthermore, with V_{DS} = 5V and back gate floating, we note clear reduction of drain current when top-gate voltage is increased. We speculate this is likely due to the injection and trapping of electrons inside the gate dielectric (Fig. 3(c)). When the top gate is biased at lower voltage, electron injection from the channel to the ZrO_2 dielectric is suppressed by the large tunneling barrier. With increased V_{TG}, this process would be greatly enhanced since the tunneling barrier is reduced. If a large proportion of electrons are trapped, the current is then reduced.

The ZrO_2/MoS_2 to-gate transistors in this work are gate-underlap transistors with large S/D access regions (Fig. 3(d)). Previous studies have found that the un-gated channel regions can lead to significant access resistance and contact resistance, thus obscuring the intrinsic performances of the top-gate MoS_2 transistors. [30] To minimize such influence and obtain the intrinsic device parameters, devices are also characterized under a large positive back-gate voltage. The positive back-gate voltage induces electron accumulation within S/D access region and thus reduce the access resistance and contact resistance. From Fig. 3(a), when a back-gate voltage of 100 V was applied, drive current was enhanced by 20 times, leading to a greater on/off current ratio of over 10^7. The current enhancement is also shown in output characteristics in Fig. 3(b), where the on-state resistance was significantly improved under a positive back-gate bias. Consequently, the maximum drive current reached ~1.4 μA/μm at V_{DS} = 5 V and V_G = 3.5 V. The extracted mobility with the back-gate biased at 100 V is 12.1 $cm^2 \cdot V^{-1} \cdot s^{-1}$, which is close to the value determined from back-gate transistor. Table 1 summarizes the device parameters from CVD monolayer MoS_2 MOSFETs using different high-*k* oxides as top-gate dielectrics.

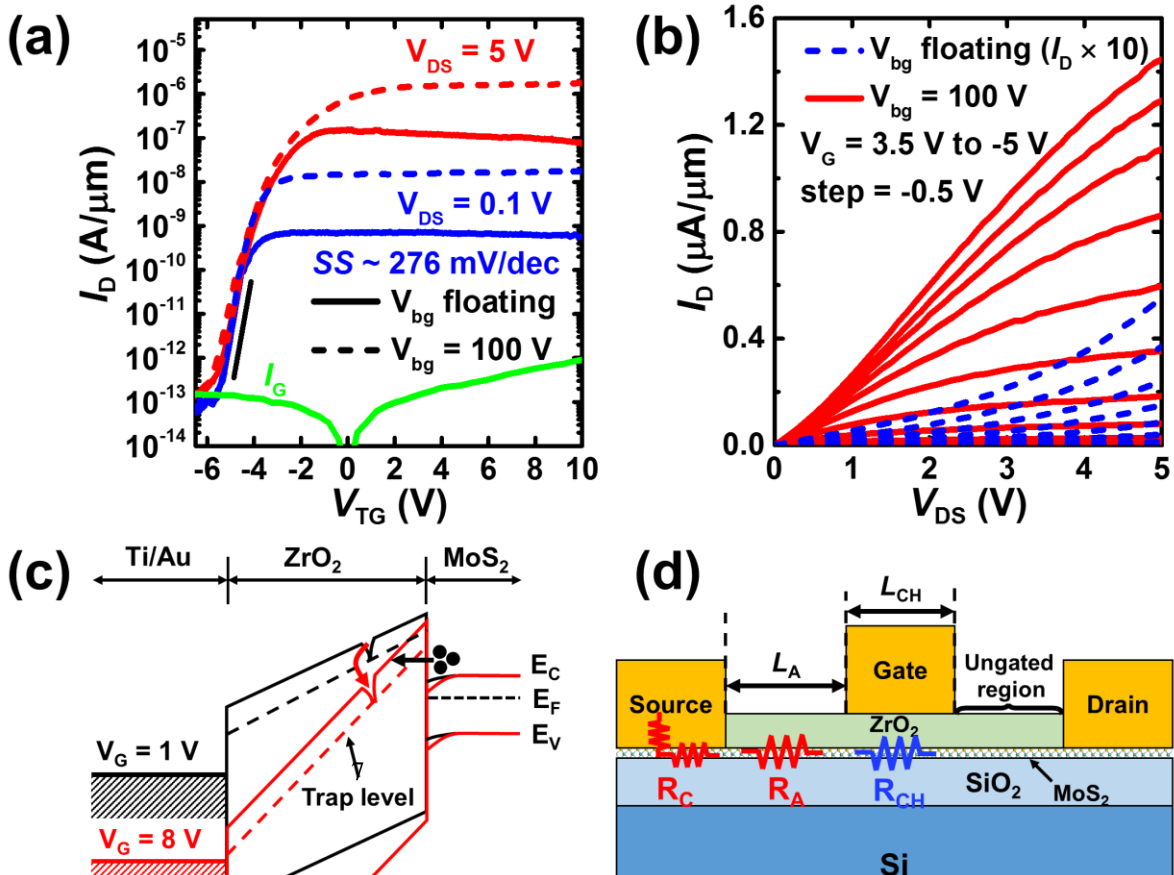

Fig. 3. (a) Transfer characteristics of ZrO_2/MoS_2 top-gate transistor (L=4 μm, W=12 μm) and (b) Output characteristics of device indicated in (a). For clarity, the drain current with back-gate floating is multiplied by 10 times. (c) Schematic band diagram of $Ti/ZrO_2/MoS_2$ MOS structure at V_{TG}= 1 V and V_{TG} =8 V. With a high top gate voltage, electron injection and trapping would occur due to the reduced tunneling barrier. (d) Schematic illustration of access resistance and contact resistance in a gate-underlap MoS_2 transistor. R_C: contact resistance, R_C: access resistance, $R_{CH:}$ channel resistance, L_A: access region length.

Table 1. The comparison of some key device parameters between different CVD monolayer MoS_2 top-gate MOSFETs.

Dielectrics	Al_2O_3	HfO_2	ZrO_2 [this work]
On/off	10^7 [19]	10^8 [35]	10^7
Off state leakage	10^{-7} μA/μm [19]	10^{-7} μA/μm [32]	10^{-7} μA/μm
Mobility	24 $cm^2V^{-1}s^{-1}$ [19]	55 $cm^2V^{-1}s^{-1}$ [33]	12 $cm^2V^{-1}s^{-1}$
Drive current	1.0 μA/μm [19]	55 μA/μm [19]	1.4 μA/μm
G_m	-	38 μS/μm [19]	2.23 μS/μm
SS	140 mV/dec [31]	110 mV/dec [32]	276 mV/dec
D_{it}	< 10^{13} cm^2eV^{-1} [34]	-	3×10^{12} cm^2eV^{-1}

To study the electrical properties of the ZrO_2/MoS_2 gate stack, gate leakage current was measured at both bias polarities in our top-gate transistor. A bias was applied to the gate terminal, with both the drain and source grounded. As shown in Fig. 4(a), the gate leakage current density J_L falls in the range 10^{-4}-10^{-2} A/cm^2 under gate biases below 10 V, which is considerably lower than that of direct ALD deposited HfO_2(28 nm)/MoS_2 gate stack [35]. The inset of Fig. 4(a) plots the J_L as a function of the electric field E_F. The breakdown field (E_{BD}) for 27 nm ALD ZrO_2 on MoS_2 is calculated to be 4.9 MV/cm, comparable to the value of ZrO_2/Al_2O_3 bilayer reported in the literature [36]. Fig. 4(b) plots the J_L-E_F curve at positive gate

biases. With $\ln(1/E_F) < -0.8$ ($V_G > 6$ V), electron injection from MoS_2 follows the Fowler-Nordheim tunneling rule, as evidenced by the linear J/E_F^2 versus $\ln(1/E_F)$ relationship. The low leakage current and high breakdown field suggest good dielectric properties of ALD ZrO_2 on MoS_2.

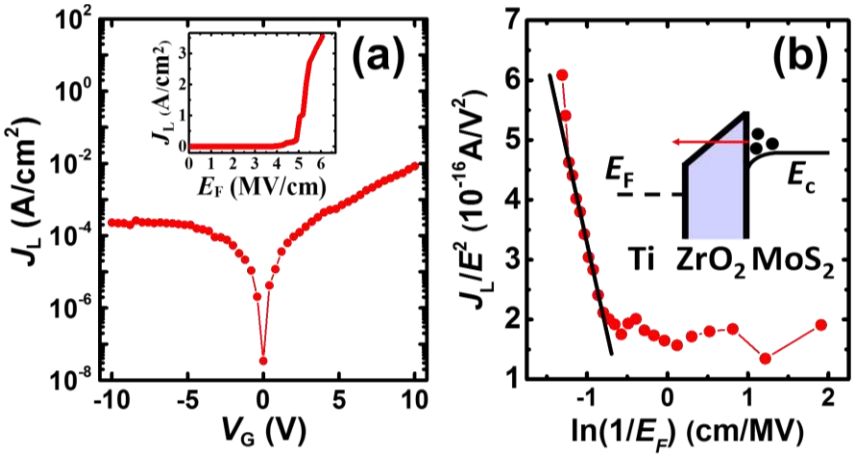

Fig. 4. (a) Leakage current characteristics of a MOSFET structure (Ti/ALD-ZrO_2/MoS_2). The inset of the figure shows the breakdown field of 27nm ALD ZrO_2 on MoS_2. (b)A J/E^2 vs $\ln(1/E)$ plot for the positive biasing condition, consistent with Fowler–Nordheim tunneling behavior.

Gate hysteresis and frequency-dependent capacitance-voltage (*C-V*) have been measured to investigate the interface quality between ZrO_2 and MoS_2. In Fig. 5(a), the gate is swept from negative to positive then back to negative voltage, with the back gate floating. The hysteresis becomes more pronounced when the sweep range is increased. This behavior, together with larger hysteresis gap at higher gate voltage, suggests a higher interface trap state density near the conduction band since the larger gate voltage, the closer the fermi level is to the conduction band. In Fig. 5(b), the *C-V* curve shows typical n-type MOS capacitor behavior, with a clear transition from depletion to accumulation when the gate voltage increases. The gate oxide capacitance C_{ox} was determined to be 790 nF/cm^2 from the maximum capacitance at 100 Hz, which corresponded to an EOT of 4.4 nm. A larger frequency dispersion was observed at the accumulation region, which also indicates a high interface trap state density close to the

conduction band. We further quantitatively extracted the interface state density using the high-low frequency method which gives the formula [37]:

$$D_{it}(V_G) = \frac{C_{ox}}{q}\left(\frac{C_{lf}/C_{ox}}{1-C_{lf}/C_{ox}} - \frac{C_{hf}/C_{ox}}{1-C_{hf}/C_{ox}}\right) \quad (1)$$

where V_G, D_{it}, q, C_{lf}, and C_{hf} represent gate voltage, interface state density, the elementary charge, low-frequency capacitance, and high-frequency capacitance, respectively. The inset to Fig. 5(b) plots the calculated D_{it} vs. gate voltage in the transition region of the CV curve (from accumulation to depletion). The D_{it} is approximately 3×10^{12} $cm^{-2}\cdot eV^{-1}$. To reduce the gate hysteresis and interface states, further studies should focus on the chemical absorption process during the ALD growth and the improvement of high-k/MoS_2 interface quality.

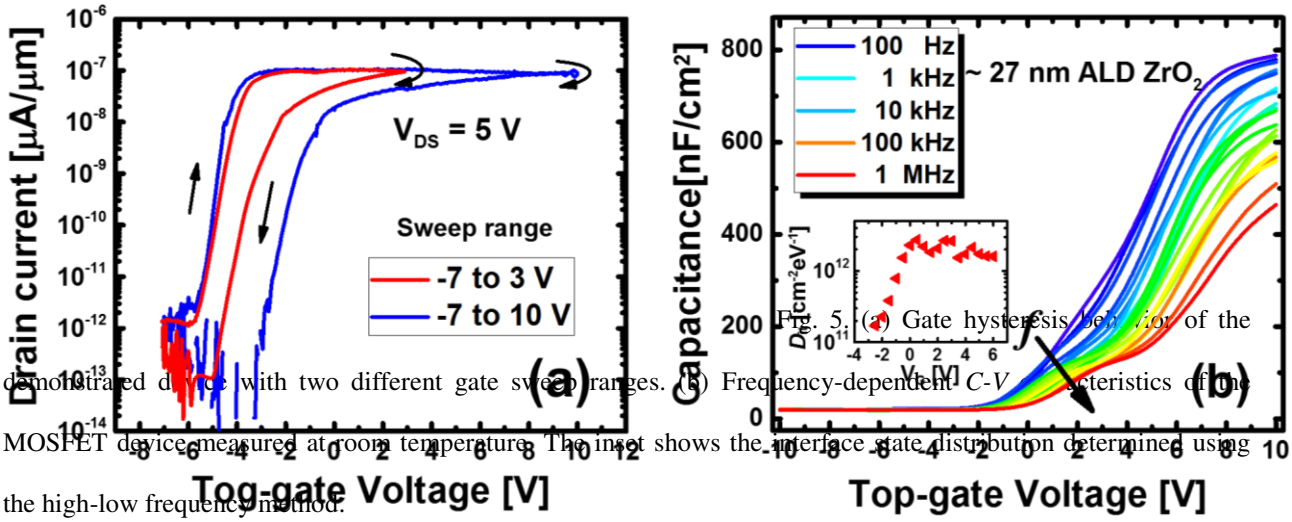

Fig. 5. (a) Gate hysteresis behavior of the demonstrated device with two different gate sweep ranges. (b) Frequency-dependent *C-V* characteristics of the MOSFET device measured at room temperature. The inset shows the interface state distribution determined using the high-low frequency method.

Further, in view of device-to-device variation, a statistical study of the key device parameters is performed to gain a comprehensive understanding of the electrical performances. The data are presented in Fig. 6. A total of 20 devices are studied with different channel lengths and widths. The average values and standard deviations are analyzed. These figures show a broad distribution of different electrical parameters which can be connected to the nonuniformity of synthesized MoS_2 film and fabrication process. The large fluctuations of gate leakage also

suggest nonuniform thickness of ZrO_2 which has been discussed in the previous part.

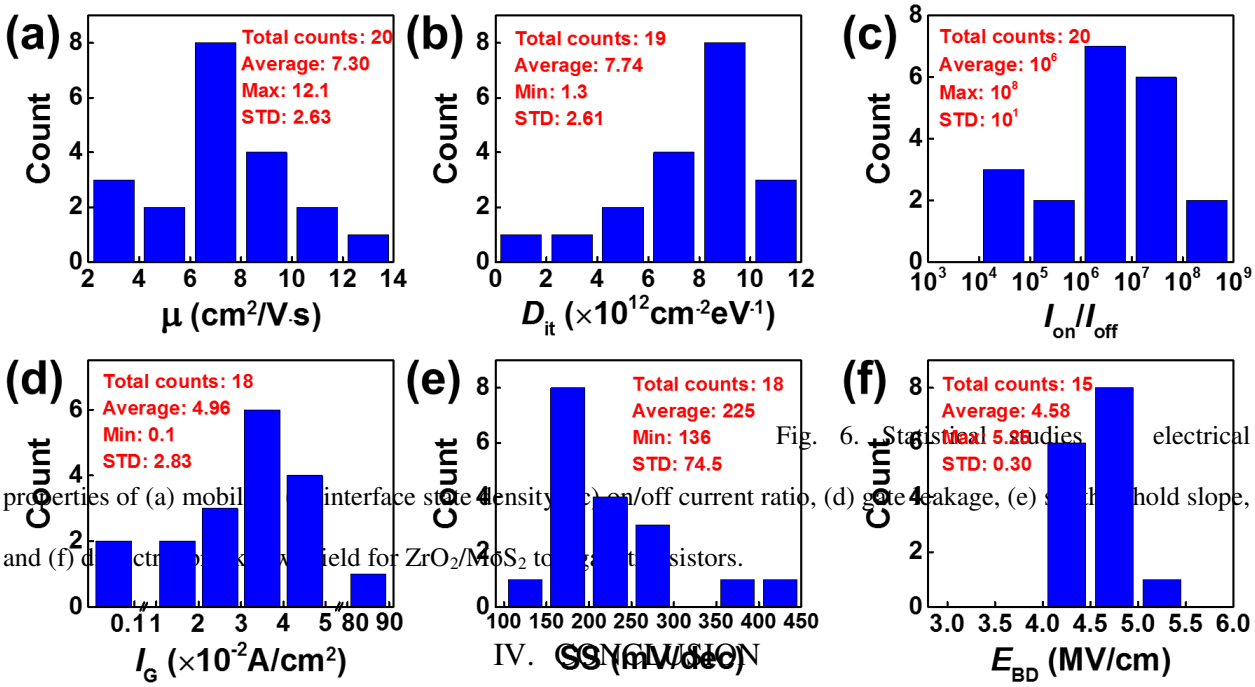

Fig. 6. Statistical studies of electrical properties of (a) mobility, (b) interface state density, (c) on/off current ratio, (d) gate leakage, (e) subthreshold slope, and (f) dielectric breakdown field for ZrO_2/MoS_2 top-gate transistors.

IV. CONCLUSION

In summary, we have experimentally demonstrated top-gate MOSFETs with monolayer MoS_2 channel and ALD ZrO_2 as gate dielectric. AFM and *I-V* studies show that ALD ZrO_2 can be directly deposited on MoS_2 with low leakage current and high breakdown field. ZrO_2 overlayer can improve the MoS_2 channel mobility. Gate hysteresis and *C-V* measurements reveal a ZrO_2/MoS_2 interface state density of about 3×10^{12} $cm^{-2}\cdot eV^{-1}$. These results suggest that ALD ZrO_2 could be a promising candidate for gate dielectric application in MoS_2-based MOSFETs.

ACKNOWLEDGMENT

This work was supported by Grant (No. 16230916) from the Research Grants Council of Hong Kong and an Initiation Grant (IGN15EG01) from HKUST. The authors would like to thank the NFF and MCPF of HKUST for technical support. Helpful discussions with L.Y. Wang and B. Lai are also appreciated.

REFERENCES

[1] Wang, Q.H., Kalantar-Zadeh, K., Kis, A., Coleman, J.N. and Strano, M.S. 2012 Electronics and optoelectronics of two-dimensional transition metal dichalcogenides. Nat. nanotechnol. **7** 699-712

[2] Radisavljevic, B., Radenovic, A., Brivio, J., Giacometti, I.V. and Kis, A. 2011 Single-layer MoS_2 transistors. Nat. nanotechnol. **6** 147-150

[3] Yoon, Y., Ganapathi, K. and Salahuddin, S. 2011 How good can monolayer MoS_2 transistors be?. Nano Lett. **11** 3768-73

[4] Das, S., Chen, H.Y., Penumatcha, A.V. and Appenzeller, J. 2012 High performance multilayer MoS_2 transistors with scandium contacts. Nano Lett **13** 100-05

[5] Kim, S., Konar, A., Hwang, W.S., Lee, J.H., Lee, J., Yang, J., Jung, C., Kim, H., Yoo, J.B., Choi, J.Y. and Jin, Y.W., 2012. High-mobility and low-power thin-film transistors based on multilayer MoS_2 crystals. *Nat. Commun*. **3** 1011

[6] Radisavljevic, B., Kis, A. 2013 Mobility engineering and a metal–insulator transition in monolayer MoS2", Nat. Mater. **12** 815-20

[7] Lembke, D., Bertolazzi, S., and Kis, A. 2015 Single-layer MoS_2 electronics. Acc. Chem. Res. **48** 100-10

[8] Azcatl, A., McDonnell, S., KC, S., Peng, X., Dong, H., Qin, X., Addou, R., Mordi, G.I., Lu, N., Kim, J. and Kim, M.J. 2014 MoS_2 functionalization for ultra-thin atomic layer deposited dielectrics. Appl. Phys. Lett., **104** 111601

[9] Yang, J., Kim, S., Choi, W., Park, S.H., Jung, Y., Cho, M.H. and Kim, H. 2013 Improved growth behavior of atomic-layer-deposited high-k dielectrics on multilayer MoS_2 by oxygen plasma pretreatment. ACS Appl. Mater. Interfaces **5** 4739-44

[10] Cheng, L., Qin, X., Lucero, A.T., Azcatl, A., Huang, J., Wallace, R.M., Cho, K. and Kim, J., 2014. Atomic layer deposition of a high-k dielectric on MoS_2 using trimethylaluminum and ozone. ACS Appl. Mater. Interfaces **6** 11834-38

[11] Jeon, T.S., White, J.M. and Kwong, D.L. 2001 Thermal stability of ultrathin ZrO_2 films prepared by chemical vapor deposition on Si (100). Appl. Phys. Lett. **78** 368-370

[12] Robertson, J. 2006 High dielectric constant gate oxides for metal oxide Si transistors. Rep. Prog. Phys. **69** 327-96

[13] Manchanda, L., Lee, W.H., Bower, J.E., Baumann, F.H., Brown, W.L., Case, C.J., Keller, R.C., Kim, Y.O., Laskowski, E.J., Morris, M.D. and Opila, R.L. 1998 Gate quality doped high K films for CMOS beyond 100 nm: 3-10 nm Al_2O_3 with low leakage and low interface states. In *Electron Devices Meeting,* 1998 *IEDM'98. Technical Digest., International*(pp. 605-608). IEEE.

[14] Balog, M., Schieber, M., Michman, M. and Patai, S. 1979 The Characteristics of Growth of Films of Zirconium and Hafnium Oxides (ZrO2, HfO2) by Thermal Decomposition of Zirconium and Hafnium β-Diketonate Complexes in the Presence and Absence of Oxygen. J. Electrochem. Soc. **126** 1203-07

[15] Wilk, G.D. and Wallace, R.M. 1999 Electrical properties of hafnium silicate gate dielectrics deposited directly on silicon. Appl. Phys. Lett. **74** 2854-56

[16] Adamopoulos, G., Thomas, S., Wöbkenberg, P.H., Bradley, D.D., McLachlan, M.A. and Anthopoulos, T.D. 2011 High-Mobility Low-Voltage ZnO and Li-Doped ZnO Transistors Based on ZrO2 High-k Dielectric Grown by Spray Pyrolysis in Ambient Air. Adv. Mater. **23** 1894-98

[17] Tao, J., Chai, J.W., Zhang, Z., Pan, J.S. and Wang, S.J. 2014 The energy-band alignment at molybdenum disulphide and high-k dielectrics interfaces. Appl. Phys. Lett. **104** 232110

[18] Amani, M., Chin, M.L., Birdwell, A.G., O'Regan, T.P., Najmaei, S., Liu, Z., Ajayan, P.M., Lou, J. and Dubey, M. 2013 Electrical performance of monolayer MoS2 field-effect transistors prepared by chemical vapor deposition. Appl. Phys. Lett. **102** 193107

[19] Sanne, A., Ghosh, R., Rai, A., Movva, H.C.P., Sharma, A., Rao, R., Mathew, L. and Banerjee, S.K. 2015 Top-gated chemical vapor deposited MoS_2 field-effect transistors on Si_3N_4 substrates. Appl. Phys. Lett. **106** 062101

[20] Desai, S.B., Madhvapathy, S.R., Sachid, A.B., Llinas, J.P., Wang, Q., Ahn, G.H., Pitner, G., Kim, M.J., Bokor, J., Hu, C. and Wong, H.S.P. 2016 MoS_2 transistors with 1-nanometer gate lengths. Science **354** 99-102

[21] Zhang, H., Chiappe, D., Meersschaut, J., Conard, T., Franquet, A., Nuytten, T., Mannarino, M., Radu, I., Vandervorst, W. and Delabie, A. 2017 Nucleation and growth mechanisms of Al_2O_3 atomic layer deposition on synthetic polycrystalline MoS_2. J. Chem. Phys. **146** 052810

[22] Obraztsov, A.N. 2009 Chemical vapour deposition: making graphene on a large scale. Nat. Nanotechnol., **4** 212-13

[23] Wang, Y., Zheng, Y., Xu, X., Dubuisson, E., Bao, Q., Lu, J. and Loh, K.P. 2011 Electrochemical delamination of CVD-grown graphene film: toward the recyclable use of copper catalyst. ACS Nano **5** 9927-33

[24] Zhan, Y., Liu, Z., Najmaei, S., Ajayan, P.M. and Lou, J. 2012 Large-area vapor-phase growth and characterization of MoS_2 atomic layers on a SiO_2 substrate. Small **8** 966-71

[25] Yongji G. Li, B., Ye, G., Yang, S., Zou, X., Lei, S., Jin, Z., Bianco, E., Vinod, S., Yakobson, B.I. and Lou, J. 2017 Direct growth of MoS_2 single crystals on polyimide substrates. 2D Mater. **4** 021028

[26] Lee, C., Yan, H., Brus, L.E., Heinz, T.F., Hone, J. and Ryu, S. 2010 Anomalous lattice vibrations of single-and few-layer MoS_2. ACS Nano, **4** 2695-700

[27] McDonnell, S., Brennan, B., Azcatl, A., Lu, N., Dong, H., Buie, C., Kim, J., Hinkle, C.L., Kim, M.J. and Wallace, R.M. 2013 HfO_2 on MoS_2 by atomic layer deposition: adsorption mechanisms and thickness scalability. ACS Nano, **7** 10354-361

[28] Yang, W., Sun, Q. Q., Geng, Y., Chen, L., Zhou, P., Ding, S.J. and Zhang, D.W., 2015 The integration of sub-10 nm gate oxide on MoS_2 with ultra low leakage and enhanced mobility. Sci Rep, **5**, 1-9

[29] Buckley, J., De Salvo, B., Deleruyelle, D., Gely, M., Nicotra, G., Lombardo, S., Damlencourt, J.F., Hollinger, P., Martin, F. and Deleonibus, S. 2005 Reduction of fixed charges in atomic layer deposited Al_2O_3 dielectrics. Microelectronic Eng. **80** 210-13

[30] Liu, H., Si, M., Deng, Y., Neal, A.T., Du, Y., Najmaei, S., Ajayan, P.M., Lou, J. and Ye, P.D. 2013 Switching mechanism in single-layer molybdenum disulfide transistors: an insight into current flow across Schottky barriers. ACS Nano, **8** 1031-38

[31] Liu, H. and Peide, D.Y., 2012 MoS_2 dual-gate MOSFET with atomic-layer-deposited Al_2O_3 as Top-Gate Dielectric. IEEE Electron Device Lett. **33**, 546-548.

[32] Wang, H., Yu, L., Lee, Y.H., Fang, W., Hsu, A., Herring, P., Chin, M., Dubey, M., Li, L.J., Kong, J. and Palacios, T., 2012, December. Large-scale 2D electronics based on single-layer MoS_2 grown by chemical vapor deposition. In *Electron Devices Meeting (IEDM),* 2012 pp. 4-6

[33] Sanne, A., Ghosh, R., Rai, A., Yogeesh, M.N., Shin, S.H., Sharma, A., Jarvis, K., Mathew, L., Rao, R., Akinwande, D. and Banerjee, S., 2015 Radio frequency transistors and circuits based on CVD MoS_2. Nano Lett. **15**, 5039-5045

[34] Yu, L., El-Damak, D., Ha, S., Ling, X., Lin, Y., Zubair, A., Zhang, Y., Lee, Y.H., Kong, J., Chandrakasan, A. and Palacios, T., 2015, December. Enhancement-mode single-layer CVD MoS_2 FET technology for digital electronics. In *Electron Devices Meeting (IEDM),* 2015 pp. 32-3

[35] Zou, X., Wang, J., Chiu, C.H., Wu, Y., Xiao, X., Jiang, C., Wu, W.W., Mai, L., Chen, T., Li, J. and Ho, J.C. 2014 Interface engineering for high-performance top-gated MoS_2 field-effect transistors. Adv. Mater., **26** 6255-61

[36] Liu, J.W., Liao, M.Y., Imura, M. and Koide, Y. 2016 High-k ZrO_2/Al_2O_3 bilayer on hydrogenated diamond: Band configuration, breakdown field, and electrical properties of field-effect transistors. J. Appl. Phys. **120** 124504

[37] Schroder, K. 2006 *Semiconductor material and device characterization* (John Wiley and Sons, Hoboken), 345